ACS OMEGA

http://pubs.acs.org/journal/acsodf

Article

Impact of Mesoporous Silica Functionalization Fine-Tuning on Antibiotic Uptake/Delivery and Bactericidal Activity

Karim Bouchmella,* Quentin Lion, Christel Gervais, and Mateus Borba Cardoso

Cite This: *ACS Omega* 2023, 8, 12154−12164

Read Online

ACCESS | Metrics & More | Article Recommendations | Supporting Information

ABSTRACT: The mesoporous SBA-15 material was surface-functionalized with amino and carboxylic acid groups and used as a platform to investigate the interaction of these chemical groups with tetracycline, kanamycin, and ampicillin antibiotics. The interactions between the antibiotic and the functionalized surfaces were characterized using two-dimensional ^{1}H-^{13}C HETCOR CP MAS and FTIR spectroscopy and indicated that $-COO^{-}$ NH_3^{+} bondings had been formed between chemical groups on the silica surface and drug molecules. The surface modification resulted in higher kanamycin and ampicillin loadings and a slow-release rate, and all synthesized systems showed antibacterial activity against susceptible *Escherichia coli* bacteria. Almost total death of bacteria was obtained using a few ppm of tetracycline- and kanamycin-loaded systems, whereas the ampicillin-loaded one showed lower bactericidal activity than free ampicillin.

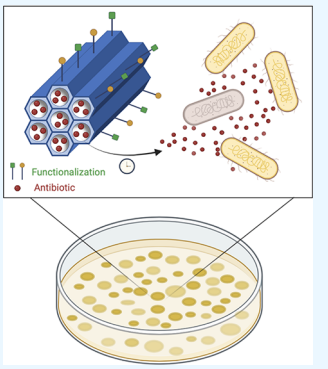

INTRODUCTION

Porous silica materials used as drug carriers have received much attention since the early 2000s.[1−5] To allow better control over drug loading and release, one of the approaches reported consists of modifying the affinity between drug and silica surface due to its capacity to be functionalized.[2] Mesoporous silica shows a high density of silanol groups, which have been successfully used to bind organic silanes that can link to the drug molecules, as described in the literature.[2,6−8] Recent reviews show that antibiotic encapsulation into porous silica is still attracting increasing attention for the preparation of drug carriers.[9,10]

There are two methods to modify the surface of mesoporous silica: co-condensation and post-synthesis grafting. In the one-pot co-condensation process, also named direct or one-pot synthesis, organosilanes are added directly to the synthesizing gel solution together with a silica source.[8] The advantages of co-condensation are uniformity in functional group distribution and high loading. However, the surfactant removal may not be complete and the organosilane may affect the pore structure and morphology of the mesoporous silica.[11] In the grafting method, the functional group is introduced after the template removal. Using this two-step process offers many possibilities for functional groups as chemically more delicate organic functionalities.[12] However, functional group distribution may not be uniform and blocking nanopores occur.[13,14] Also, co-condensed organosilicas possess functional groups connected to the silica support by two or three siloxane bonds, while only one or two siloxane bonds typically bind grafted sites.[15] As a result, the attachment of the functional groups in co-condensed silicas tends to be more stable than in grafted sites.

Characterizing the nature of drug@functionalized-silica interactions allows a better understanding of the properties and, therefore, better control of the release rate. Solid-state NMR has proved to be an adequate tool to characterize such interactions as it allows to investigate not only the local environment of nuclei of the drug (through various NMR interactions, such as the chemical shift) but also the longer-range connectivities between the organic molecule and the inorganic surface (either through-bond or through-space interaction).[16] For example, confinement of ibuprofen in MCM-41 (Mobil Composition of Matter number 41) matrices was studied in-depth by NMR using 1D (MAS-J-INEPT, CP MAS, Magic Angle Spinning - J - Insensitive Nuclei Enhanced by Polarization Transfer, Cross Polarization Magic Angle Spinning) and 2D (MAS-J-HMQC, Magic Angle Spinning - J - Heteronuclear Multiple Quantum Coherence) experiments, which allowed evidence of several physical states of ibuprofen.[17,18] In parallel, using FTIR spectroscopy, Fiorilli et al. showed that the carboxylic groups of the functionalized SBA-15 (Santa Barbara Amorphous-15) material react reversibly at room temperature with ammonia, forming carboxylate species (COO^{-}) and ammonium ions (NH_4^{+}).[19]

Received: December 19, 2022
Accepted: March 8, 2023
Published: March 22, 2023

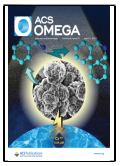

Thereafter, Tang et al. investigated the formation of the same ionic interactions between famotidine amino groups and carboxylic acid groups of the functionalized MSU (Montana State University) material.[20] Similar results were obtained by other authors with the amino-functionalized SBA-15 material and amoxicillin.[21] FTIR spectroscopy was also used to exhibit hydrogen bonding interactions between tetracycline molecules and amino-modified SBA-15 surface.[22]

Within this context, the correlation between the drug and the silica carrier in intimate interaction, and the physiological environment or the presence of pathogens remains unveiled. Thus, it is imperative to enrich the scientific debate on therapeutic strategies of antibiotics against pathogenic bacteria by trying to address fundamental questions. First, it is needed to rationally play with the interactions of drugs and carriers in a given fashion where properties can be tailored to achieve the desired property. Second, it is critical to establish a correlation between these tailored-generated interactions and the ultimate bactericidal activities at ultra-low concentrations (ppm).

Herein, we used mesoporous SBA-15 silica as a carrier and three antibiotics as drug models. Tetracycline hydrochloride, kanamycin sulfate, and ampicillin sodium are antibiotics whose structures exhibit hydroxyl, amino, and carboxylate groups (see the Supporting Information, Figure S1). Using one-pot and two-step synthesis, a specific functionalization of the SBA surface (with amino and carboxylic acid groups) was achieved to increase the drug loading capacity of the carrier. Solid-state NMR and FTIR spectroscopies were used to investigate the drug@carrier interactions. Finally, the antibacterial activity of drug@carrier systems was tested against susceptible Gram-negative *Escherichia coli* bacteria. It is the first study to investigate the effect of a specific functionalization of mesoporous silica on the uptake and delivery of various antibiotics while establishing a clear correlation between the ultimate bactericidal activity and the properties of the synthesized drug@carrier systems.

MATERIALS AND METHODS

Materials. Pluronic P123 (poly(ethylene glycol)-block-poly(propylene glycol)-block-poly(ethylene glycol), average Mn ∼ 5800), tetraethylorthosilicate (TEOS, 98%), sodium fluoride (≥99%), 3-(triethoxysilyl)propyl isocyanate (95%), (3-aminopropyl)triethoxysilane (≥98%), ammonium hydroxide (28−30%), tetracycline hydrochloride (T), kanamycin sulfate (K), ampicillin sodium (A), and Mueller Hinton Broth (MHB) medium were purchased from Sigma-Aldrich. Absolute ethanol and fluorescamine were obtained from Merck. All reagents were used as purchased without further purification. Water used in all procedures was obtained from a water purification system (PURELAB from ELGA) and had a measured resistivity of 18.2 MΩ.cm.

SBA-15 Material Synthesis. *Synthesis of the SBA-15 Carrier (SBA).* Pluronic P123 (4.68 g, 0.8 mmol) was dissolved in an aqueous HCl solution (pH 1.5, 150 mL), and TEOS (11.79 g, 56 mmol) was added to the solution. The resulting mixture was stirred until a clear solution was obtained, and then NaF (82 mg, 1.9 mmol) was added to activate the silicon center and induce polycondensation. After aging under regular stirring for 72 h at 60 °C, the resulting powder was removed by filtration. Then, the surfactant was removed by Soxhlet extraction with hot ethanol for 72 h. The solid product was dried at 80 °C under vacuum.

Synthesis of the Amino-Functionalized SBA-15 Material (SBA-NH_2). 0.5 g of SBA and 600 μL of (3-aminopropyl)-triethoxysilane (2.6 mmol) in 50 mL of ethanol was stirred for 30 min at room temperature. Ammonium hydroxide solution (5 mL) was added to the mixture. After stirring 1 day at room temperature, the resulting solution was filtered. The precipitate was washed three times with 20 mL of ethanol and dried under ambient air.

Synthesis of the Carboxylic Acid-Functionalized SBA-15 Material (SBA-CO_2H). The carboxylic acid-functionalized SBA material preparation was partially based on the previously published synthesis route.[23] Pluronic P123 (4.45 g, 0.8 mmol) was dissolved in an aqueous solution of HCl (pH 1.5, 150 mL). TEOS (12.3 g, 59 mmol) was added to 3-(triethoxysilyl)-propyl isocyanate (1.38 g, 6 mmol). This mixture was stirred until a clear solution was obtained, and then NaF (64 mg, 1.5 mmol) was added. After stirring for 3 days at 60 °C, the resulting powder was filtered off, and the surfactant was removed by Soxhlet extraction with hot ethanol for 24 h. The recovered solid was dried at 70 °C under vacuum. The obtained sample was denoted as SBA-CN. Propyl carboxylic acid-functionalized SBA-CO_2H was prepared by heating SBA-CN (4 g, 6.1 mmol) under reflux with an aqueous solution of H_2SO_4 (100 mL, 50%) at 120 °C over 12 h. The SBA-CO_2H solid product was recovered by filtration, washed several times with water, ethanol, acetone, and diethyl ether, and then dried at 70 °C under vacuum.

Drug Loading Procedure (T@SBA, K@SBA-CO_2H, and A@SBA-NH_2). Drugs were dissolved in distilled water to form a 40 mg/mL solution. 40 mg of the carrier was impregnated with 2 mL of the drug solution to perform the loading procedure. The mixture was stirred at room temperature for 72 h to reach the equilibrium state. After the impregnation, the sample was collected by centrifugation. Then, to remove the unabsorbed drug, the sample was washed with distilled water, ethanol, and acetone and dried under ambient air.

Drug Release Experiments. Standard stock solutions with different concentrations of T were used to obtain a calibration curve employed in the quantitative determination of T leakage by ultraviolet−visible spectroscopy (UV−vis). The T@SBA material (1 mg) was placed in a buffer solution (1 mL) of simulated body fluid (a phosphate buffer solution, PB, 0.1 M, pH 7.4) incubated at 37 °C under stirring with 200 rpm. At predetermined time intervals, the suspension was centrifuged (10,000 rpm, 10 min), and 20 μL was collected from the supernatant and analyzed by UV−vis. The solid residue was redispersed, and 20 μL of the buffer solution was added back to the original material suspension. The released concentration as a function of time was analyzed by UV−vis using an Agilent 8453 spectrophotometer at a wavelength of 275 nm. For each material, the experiments were conducted in triplicate.

In this study, a spectrofluorometric method based on the reaction of K and A with fluorescamine was used to analyze the amount of released drug.[24] A fluorescence spectrophotometer was used to record fluorescence spectra and measurements. Standard solutions of 1 mg/mL fluorescamine, K, and A were freshly prepared and used to obtain a calibration curve for each drug.

K@SBA-CO_2H and A@SBA-NH_2 materials (1 mg) were placed in PB solution (1 mL, 0.1 M, pH 7.4) incubated at 37 °C under stirring at 200 rpm. At predetermined time intervals, the suspension was centrifuged (10,000 rpm, 10 min) and 20 μL of analyte solution was collected from the supernatant and

https://doi.org/10.1021/acsomega.2c08065
ACS Omega 2023, 8, 12154−12164

analyzed. The solid residue was redispersed, and 20 μL of the buffer solution was added back to the original material suspension. To analyze the released-drug concentration as a function of time, 20 μL of analyte solution was mixed with 190 μL of PB solution (0.1 M, pH 7.4) and 90 μL of fluorescamine solution (1 mg/mL). The fluorescence intensity was measured against a blank (210 μL of PB solution mixed with 90 μL of fluorescamine solution) with excitation at 392 nm and emission at 478 nm. For each material, the experiments were conducted in triplicate.

Characterization of the Materials. Transmission electronic microscopy (TEM) was carried out in a JEOL 2100 (0.25 nm point-to-point resolution) with an accelerating voltage of 200 kV for TEM acquisitions. Thermogravimetric analysis (TGA) measurements were carried out under air from 20 to 800 °C (5 °C/min) on a Perkin-Elmer Thermogravimetric Analyzer Pyris 1 TGA. The nitrogen adsorption−desorption isotherms were obtained at 77 K using a TriStar II 3020 (Micromeritics) instrument. The specific surface area was obtained according to the standard BET (Brunauer−Emmett−Teller) method in the 0.05−0.30 P/P0 range. The total micropore volume of the sample was estimated using *t*-plot analysis. The samples were degassed at 80 °C for 4 h under vacuum before the measurements. ^{29}Si and ^{13}C solid-state NMR spectra of functionalized SBA-15 materials were recorded on a Varian VNMRS 300 solid spectrometer with a magnetic field strength of 7.05 T equipped with a 3.2 mm MAS probe at 6 kHz as a spinning rate. ^{29}Si and ^{13}C CP MAS NMR experiments were acquired with a 5 s pulse sequence repetition delay and a 5 μs $\pi/2$ (^{1}H) pulse duration. Contact times of 5 and 3 ms were used for ^{29}Si and ^{13}C, respectively. Both nuclei were referenced to tetramethylsilane (TMS). ^{1}D ^{13}C CP MAS and 2D HETCOR ^{13}C-{^{1}H} CP MAS (two-Dimensional HETeronuclear CORrelation ^{13}C-{^{1}H} Cross Polarization Magic Angle Spinning) NMR spectra of the three antibiotics, pure and encapsulated, were recorded on a Bruker Avance 700 spectrometer (field = 16.4 T, ν_0(^{1}H) = 700.14 MHz, ν_0(^{13}C) = 176.08 MHz) using a 4 mm Bruker MAS probe spinning at 10 kHz. The structural organization of the materials was investigated through the small-angle X-ray scattering (SAXS) technique. The SAXS experiments were carried out on the D1B beamline at the LNLS using a wavelength λ = 1.488 Å. The X-ray beam was monochromatized with a multilayer monochromator and collimated by a set of slits defining a pin-hole geometry. The sample-to-detector distance was 3000 mm, covering a scattering vector q ($q = (4\pi/\lambda)\sin\theta$; 2θ = scattering angle) ranging from 0.06 to 1 nm^{-1}. All solid measurements were performed at room temperature. Silver behenate powder was used as a standard to calibrate the sample-to-detector distance, the detector tilt, and the direct beam position. Transmission, dark current, and empty cell corrections were performed on the 2D image before further data processing. The isotropic scattering patterns were radially averaged. The UV−vis absorption spectra were performed using a UV−vis Agilent 8453 spectrophotometer. A PerkinElmer EnSpire Multimode Plate Reader fluorescence spectrophotometer with a xenon flash lamp, grating monochromators for excitation and emission, and an Agilent Cary Eclipse recorder was used to record fluorescence spectra and measurements. The biological experiments were performed in 96-well microplates, and the Multiskan FC Microplate Photometer (Fisher Scientific), equipped with an optical filter of 600 nm, was used to measure the bacterial turbidity indicating bacteria growth during the time.

The NMR parameters were calculated within Kohn−Sham DFT using the Quantum ESPRESSO code,[25] on published crystalline structures of tetracycline hydrochloride (CCDC 153890) and kanamycin monosulfate monohydrate (CCDC 1198235) after relaxation of the proton positions. The PBE-generalized gradient approximation[26] was used, and the valence electrons were described by norm-conserving pseudopotentials[27] in the Kleinman−Bylander form.[28] The shielding tensor was computed using the Gauge Including Projector Augmented Wave (GIPAW) approach.[29]

Biological Experiments. *Incubation Experiments with E. coli Bacteria.* A single colony of susceptible *E. coli* (DH5α) was taken from an Agar plate grown for 18−20 h at 37 °C and transferred into 5 mL of MHB medium. The bacterial suspension was incubated overnight at 37 °C under vigorous shaking (200 rpm). The bacterial suspension was aseptically transferred to a sterile polypropylene tube to start three washes with a NaCl solution (0.85% m/v). First, to the 5 mL bacteria suspension was added 5 mL of NaCl solution. The suspension was centrifugated at 4000 rpm (Himac, CR20B2) for 10 min. The pellet was resuspended in 10 mL of NaCl solution. After centrifugation (4000 rpm for 10 min), the pellet was then resuspended and centrifuged in the same conditions. The pellet was resuspended in 2 mL of PB (pH 7.4). The bacterial growth was determined by measuring the optical density (OD) at 600 nm with an Ultrospec 3000 spectrometer from Pharmacia Biotech. A dilution was realized to obtain a colony-forming unit (CFU) concentration of 2 × 10^6 CFU/mL on MHB medium.

For each material (SBA-15-type systems and drugs), a 1 mg/mL material suspension was prepared in water. The suspension was sonicated for 10 min to disperse the material. A dilution was realized to obtain a stock solution of 100 μg/mL on an MHB medium. To measure the growth rate of *E. coli* in the presence of different concentrations of each material, 125 μL of the bacterial suspension (with a concentration of 2 × 10^6 CFU/mL) was added to a 96-well plate containing the desired volume of 100 μg/mL of MHB stock solution and a sufficient quantity of MHB medium to obtain 250 μL total volume. Wells lacking bacteria were used as negative controls, and wells with bacteria and without materials (SBA-15-type systems and drugs) were used as positive controls. The plates were then sealed with a cap and incubated at 37 °C in a microplate photometer. Absorbance was measured at 600 nm every 10 min, with 15 s of shaking every 2 min and 5 s of settle time before each measurement. Measurements were collected for 20 h. For all the materials and controls, the experiments were conducted in triplicate. To obtain the percentage of OD, the three tests' average was compared to that of the positive control as

$$\%\text{of OD} = B/A \times 100$$

where A is the average OD in the positive control sample and B is the average OD in the test sample.

RESULTS AND DISCUSSION

Synthesis and Composition of Functionalized SBA-15 Materials. SBA-15 materials were prepared following the described procedure that consists in the hydrolysis and polycondensation of TEOS in acidic media and the presence of surfactant (Pluronic P123) as a structure-directing agent.[30]

https://doi.org/10.1021/acsomega.2c08065
ACS Omega 2023, 8, 12154−12164

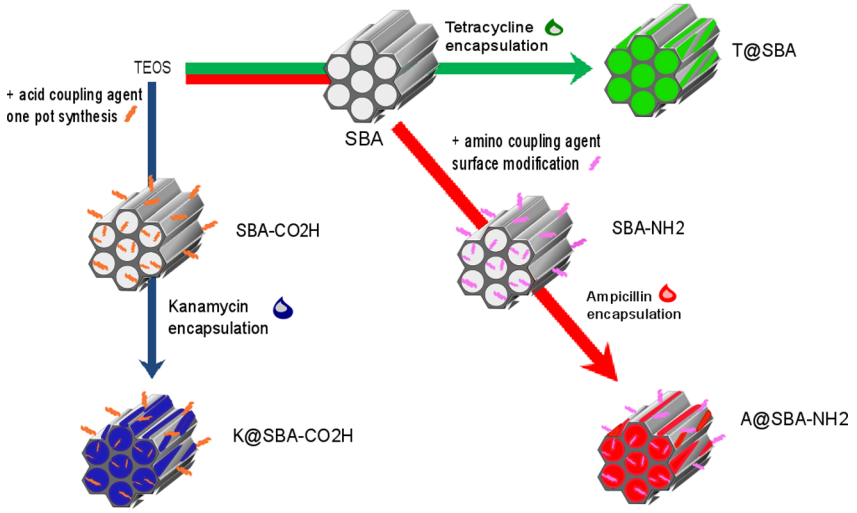

Figure 1. Schematic representation of the organic groups and drug-loaded SBA-15-type systems syntheses. TEOS means tetraethylorthosilicate (formally named tetraethoxysilane). The functionalization step consisted in the carboxylic acid group grafting (called SBA-CO_2H) by mixing TEOS with 3-(triethoxysilyl)propyl isocyanate, followed by acid hydrolysis. The other functionalization consisted in the amino group grafting (named SBA-NH_2) by mixing the SBA material with (3-aminopropyl)triethoxysilane. The overall material yield was better than 80% in all cases. Finally, antibiotics were adsorbed into materials by impregnating the specified drug with an aqueous solution. T, K, and A mean, respectively, tetracycline, kanamycin, and ampicillin.

The unfunctionalized SBA-15 material (named SBA) was obtained after removing the surfactant by extraction with ethanol in a Soxhlet apparatus (Figure 1).

In a second step synthesis, the amino-modified SBA-15 material (SBA-NH_2) was obtained by mixing the SBA material with (3-aminopropyl)triethoxysilane in ethanol. The preparation of carboxylic acid-modified SBA (named SBA-CO_2H) involves a one-pot synthesis of cyanide-functionalized hybrid material followed by treatment with sulfuric acid.[20,23,31] Finally, impregnation with an aqueous solution of tetracycline hydrochloride (T), ampicillin sodium (A), and kanamycin sulfate (K) were carried out on the unfunctionalized SBA, amino-functionalized and carboxylic acid-functionalized carriers to obtain the drug-loaded systems (T@SBA, A@SBA-NH_2, and K@SBA-CO_2H, respectively).

Characterization of Functionalized SBA-15 Materials. TEM images show that the silica material exhibits a well-ordered hexagonal array (Figure 2A) and large open pores (Figure 2B) with a common stick-like shape of SBA-15.

Moreover, it was verified that the morphology of the functionalized materials was not disrupted by the introduction of organic groups (Figure S2), whose loadings were determined by TGA. The organic groups' weight loading of the carboxylic acid-modified SBA (SBA-CO_2H) and amino-modified SBA (SBA-NH_2) are 8 and 9 wt %, respectively (Figure 2C). The weight loss of the organic part in the hybrid framework co-occurs with the residual P123 surfactant (Table S1). The quantification protocol used here is fully described in the Supporting Information.

As summarized in Figure 2D,E, SBA-CO_2H had similar textural properties (SSA and Dp derived from the nitrogen adsorption−desorption isotherm and pore size distribution curve, respectively) to that of SBA. In contrast, SBA-NH_2 had a much lower surface area and higher pore diameter than both. This confirms that the $-NH_2$ functional group is located mainly on the outer surface. In this study, the two methods used to modify SBA materials chemically influenced the textural properties. In terms of specific surface area, the one-pot synthesis (co-condensation) is much more advantageous than post-synthesis grafting.[32] The ^{29}Si CP-MAS NMR spectra of the SBA-15-type materials display three signals at −91, −102, and − 111 ppm attributed to the Q^2, Q^3, and Q^4 environments, respectively (Figure 2F-1,F-3,F-5). The functionalization of the SBA material by the coupling agents containing the propyl spacer was confirmed by the presence of T^2 and T^3 substructures at around respectively −60 and − 70 ppm (Figure 2F-3,F-5). The ^{13}C CP-MAS NMR spectrum of the SBA material (Figure 2F-2) indicates the presence of the residual Pluronic P123 surfactant (confirmed by TGA, see Table S1). The spectrum displays four signals (73, 71, 60, and 18 ppm) assigned to the poly(ethylene glycol) and poly(propylene glycol) units and an additional one at 163 ppm attributed to carbonyl resonances of ester and amide groups of the Pluronic P123 surfactant.[33]

The ^{13}C NMR spectra of the SBA-CO_2H and SBA-NH_2 materials (Figure 2F-4,F-6) clearly showed that the functionalization with propyl spacer coupling agents was successfully obtained. The signal at 10 ppm corresponds to the methylene carbon group directly bonded to the silicon atom (C^a). The signal at around 20 ppm was attributed to the second methylene carbon (C^b) of the ≡Si-C^aH_2-C^bH_2-C^cH_2-X modifying agent (where X represents CO_2H or NH_2). Signals for the methylenes adjacent to the functional carboxylic and amino groups (C^c) are present at 36 and 44 ppm, respectively. The signal for the $-CO_2H$ group is present at 177 ppm (Figure 2F-4). Furthermore, it was confirmed by the absence of the resonance at 120 ppm assigned to the −C≡N functionality that no unreacted cyano groups remained on the sample surface.[23,31,34,35] The residual P123 surfactant and unidentified impurity remained in SBA-CO_2H and SBA-NH_2 carriers as indicated by one and two asterisks, respectively (Figure 2F-4,F-6).

After drug impregnation, the total drug quantification of the resulting solids was determined by TGA, as reported in Figure 3A.

https://doi.org/10.1021/acsomega.2c08065
ACS Omega 2023, 8, 12154−12164

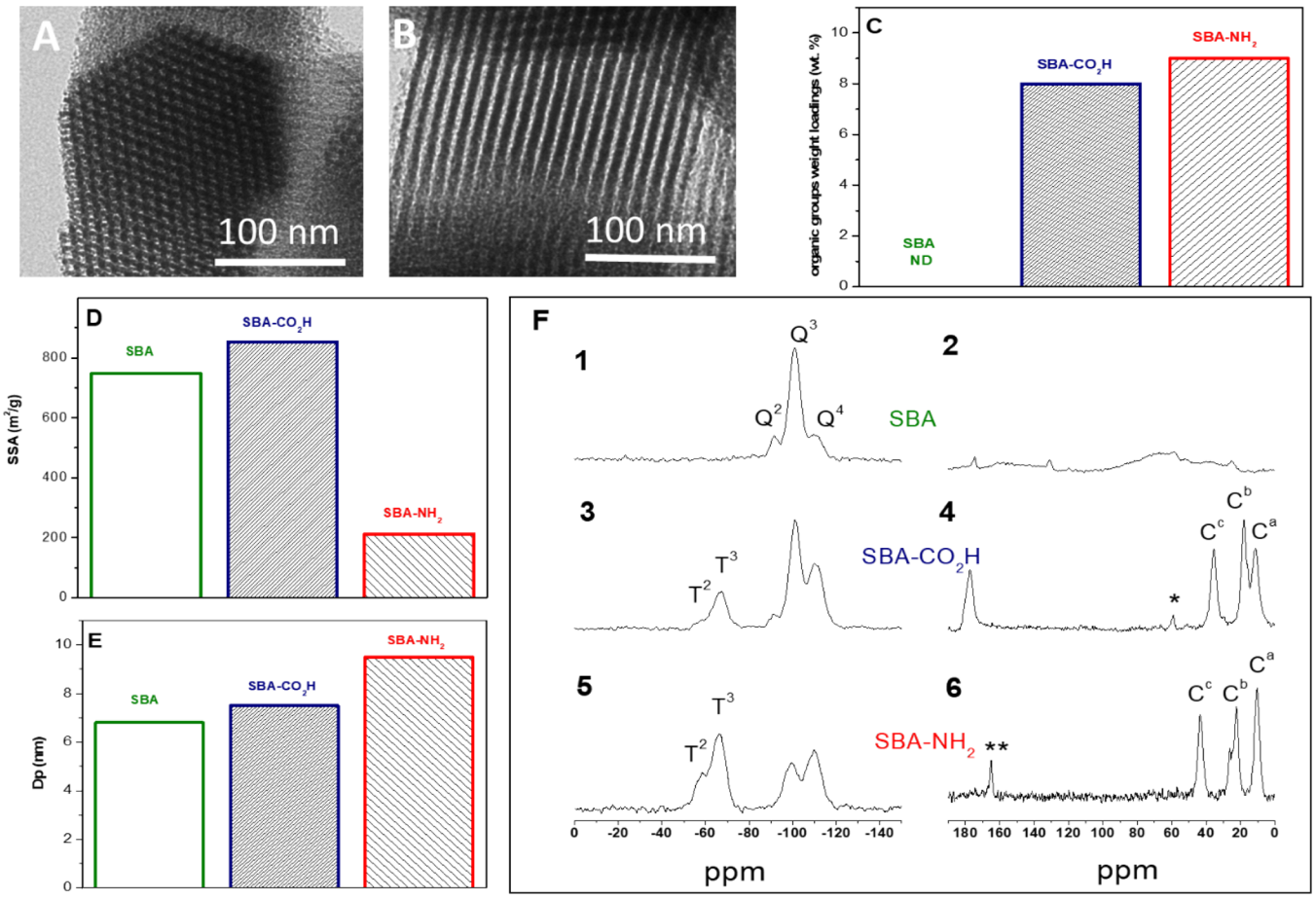

Figure 2. (A, B) TEM images of the SBA sample. (C) Weight percentage of organic groups determined by TGA (TGA weight loss was carried out between 150 and 800 °C). (D) BET surface area (in m^2/g). (E) Pore diameter (in nm, obtained from the equation: $4 \times V/SBET$ with V as single-point adsorption total pore volume of pores at $P/P0 = 0.98$). Textural properties of the samples were measured by N_2 adsorption−desorption measurements. (F) (1, 3, and 5) ^{29}Si and (2, 4, and 6) ^{13}C CP-MAS NMR of (1 and 2) SBA, (3 and 4) carboxylic acid-functionalized (SBA-CO_2H), and (5 and 6) amino-functionalized (SBA-NH_2) carriers. The connectivity of the various silicon sites can be identified by using ^{29}Si NMR and specified by the substructures T^n and Q^n, where n is the number of siloxane bonds linking the Si site to the silica framework. T^n is used for [SiR] groups with one covalent bond to carbon and up to three siloxane bonds, and Q^n sites possess no Si−C bonds. C^a, C^b, and C^c are localized in the propyl spacer: ≡Si-C^aH$_2$-C^bH$_2$-C^cH$_2$-X (where X represents CO_2H or NH_2). The residual P123 surfactant and unidentified impurity remained in the studied samples as indicated by one and two asterisks, respectively.

The weight loss of the drug quantification coincides with the organic part in the hybrid framework. The quantification protocol is fully described in the Supporting Information. Table S1 summarizes the total weight loss of all the synthesized samples. We experimented the impregnation of T, K, and A on each carrier. This preliminary investigation showed that the drug loading depends on the interaction of the drug with the carrier. According to Table S1, the most efficient carrier for T, K, and A is unfunctionalized SBA, carboxylic acid-modified SBA, and amino-modified-SBA, respectively. A T loading of 20 wt % was obtained for the unfunctionalized SBA, and this result correlates well with the data found in the literature.[22] The higher drug loading for SBA-CO_2H was 16.5 wt % of K and 17.4 wt % of A for the SBA-NH_2 carrier.

As expected, after drug impregnation, the SBA and SBA-CO_2H carriers showed a significant decrease in the surface area. Surprisingly, A adsorption on the amino-modified SBA carrier remained in the same order of magnitude as the corresponding parent SBA-NH_2 (Figure 3B). This can be explained by a large amount of A adsorbed on the external surface of the SBA-NH_2 carrier. For the T@SBA and A@SBA-NH_2 samples, there is no reduction in average pore diameter compared to the corresponding silica parent, suggesting that most of the drug was adsorbed on the outer surface (Figure 3C). The average pore diameter changes drastically for SBA-CO_2H after K impregnation, and we attribute this result to the smaller pore blockage while the larger ones remain accessible for N_2 physisorption.[36]

Figure 3D shows the SAXS patterns for the drug-loaded SBA materials. All samples presented similar SAXS profiles where higher-order reflections were found, indicating long-range ordering of the porous system. These materials exhibited the characteristic Bragg reflection sequence for a 2D hexagonal ordering (1: 31/2: 2: 71/2, etc.), which were indexed to the (100), (110), and (200) crystallographic planes.[37] As expected, the presence of crystalline drugs was not detected.

Investigation of Drug@Carrier Interactions. ^{13}C CP MAS NMR spectra of the three antibiotics after loading in SBA materials (Figure 4a) show a significant broadening of the lines, particularly when compared to the spectra of pure kanamycin sulfate and tetracycline hydrochloride exhibiting very narrow lines, probably due to a good crystallinity. A tentative assignment of the ^{13}C signals of T and K is proposed in the SI (Figures S3 and S4) based on the DFT calculation of

https://doi.org/10.1021/acsomega.2c08065
ACS Omega 2023, 8, 12154−12164

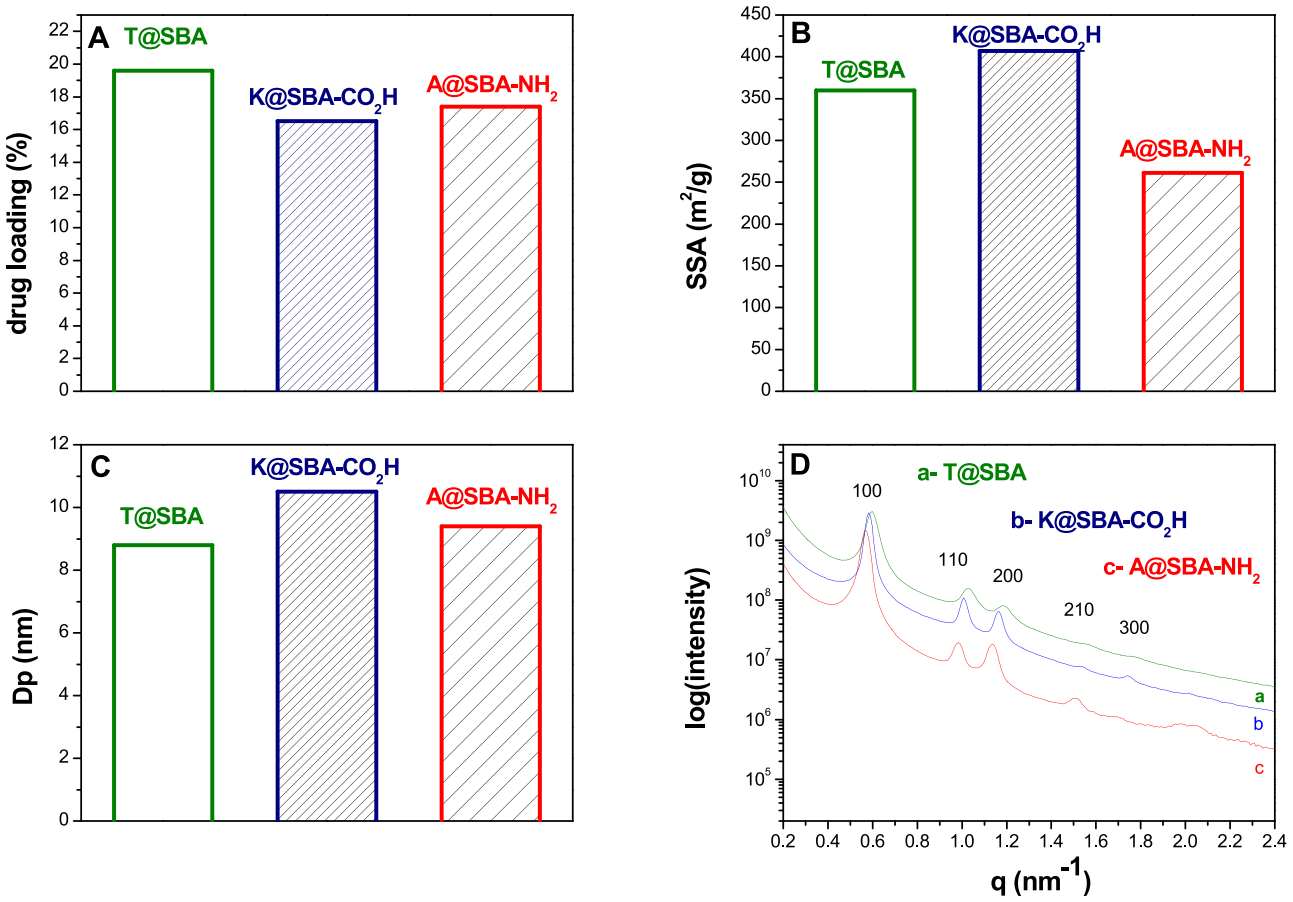

Figure 3. (A) Total drug quantification (in weight percentage) was determined by TGA measurements (between 150 and 800 °C). (B) BET surface area (in m^2/g). (C) Pore diameter (in nm, obtained from the equation: $4 \times V/SBET$ with V as single-point adsorption total pore volume of pores at $P/P0 = 0.98$). Textural properties were measured by N_2 adsorption−desorption measurements. (D) SAXS scattering patterns of drug-loaded systems.

NMR parameters computed on the published structures of these compounds (Cf Methods). The proposed attributions are consistent with those observed in solution for tetracycline hydrochloride[38] and kanamycin.[39] In the case of ampicillin sodium, assignment of the ^{13}C CP MAS NMR spectrum is proposed (Figure S5) based on a previously reported solid-state NMR study of ampicillin.[40] When comparing, for instance, the spectra of K and K@SBA-CO_2H, apart from the broadening of the lines, some signals present in the pure antibiotics (like the intense one at ∼93 ppm) seem to disappear or be shifted after loading. This has already been observed in the case of the adsorption of tetracycline on zeolite beta[41] and can indicate the interaction between the organic molecule and the functionalized SBA surface. To investigate these possible interactions in detail, two-dimensional ^1H-^{13}C HETCOR CP MAS experiments were recorded and compared for pure and loaded A (Figure 4b) and K (Figure 4c). Interestingly, loaded A@SBA-NH_2 shows an intense cross-peak between the carbon signal at ∼43 ppm (assigned to the methylene adjacent to the functional amino group (C^c)) and a composite proton signal centered around 7.5 ppm. The latter can be the superimposition of the amine signal of SBA-NH_2 and protons signals of ampicillin (such as aromatic or amine), suggesting proximity between the antibiotic and the functionalized surface. Similarly, loaded K@SBA-CO_2H shows an interesting cross-peak between the COO carbon of the functionalized surface around 180 ppm and protons at ∼5.8 ppm expected for an OH or amine group of kanamycin (Figure S3).

Complementarily to solid-state NMR experiments, further evidence of the interactions that can occur between the drug and the carrier was studied by FTIR spectroscopy. FTIR spectra of free drugs and SBA carriers before and after drug loading are shown in Figure 5.

All the carriers possess a broader band at around 1100 cm^{-1}, attributed to the Si−O−Si asymmetric stretching vibration characteristics of a condensed silica network (Figure 5A,C,E).[42] The broad peak at 3400 cm^{-1} is attributed to the −OH stretching vibration mode. The band at 1640 cm^{-1} in these samples is due to the −OH deformation band, and the sharp band around 950 cm^{-1} is associated with the Si−OH groups.[43] The characteristic absorbance peaks of the triblock copolymer, corresponding to C−H stretching (around 2900 cm^{-1}) and bending vibrations (around 1400 cm^{-1}) or to the carboxyl group (−C=O) stretching vibration (around 1640 cm^{-1}), are not observed.[43]

Compared to the SBA carrier spectrum (Figure 5A), the functionalization with propyl groups results in the appearance of the bands around 2900 cm^{-1} (Figure 5C,E), which are attributed to C−H vibrations of propyl anchored on the surface of mesoporous support.[44]

As shown in Figure 5B, the assignment of the main bands related to FTIR spectra of T can be found at 1675 cm^{-1} for C=O, at 1620 cm^{-1} for C=C stretching of the aromatic ring, at

https://doi.org/10.1021/acsomega.2c08065
ACS Omega 2023, 8, 12154−12164

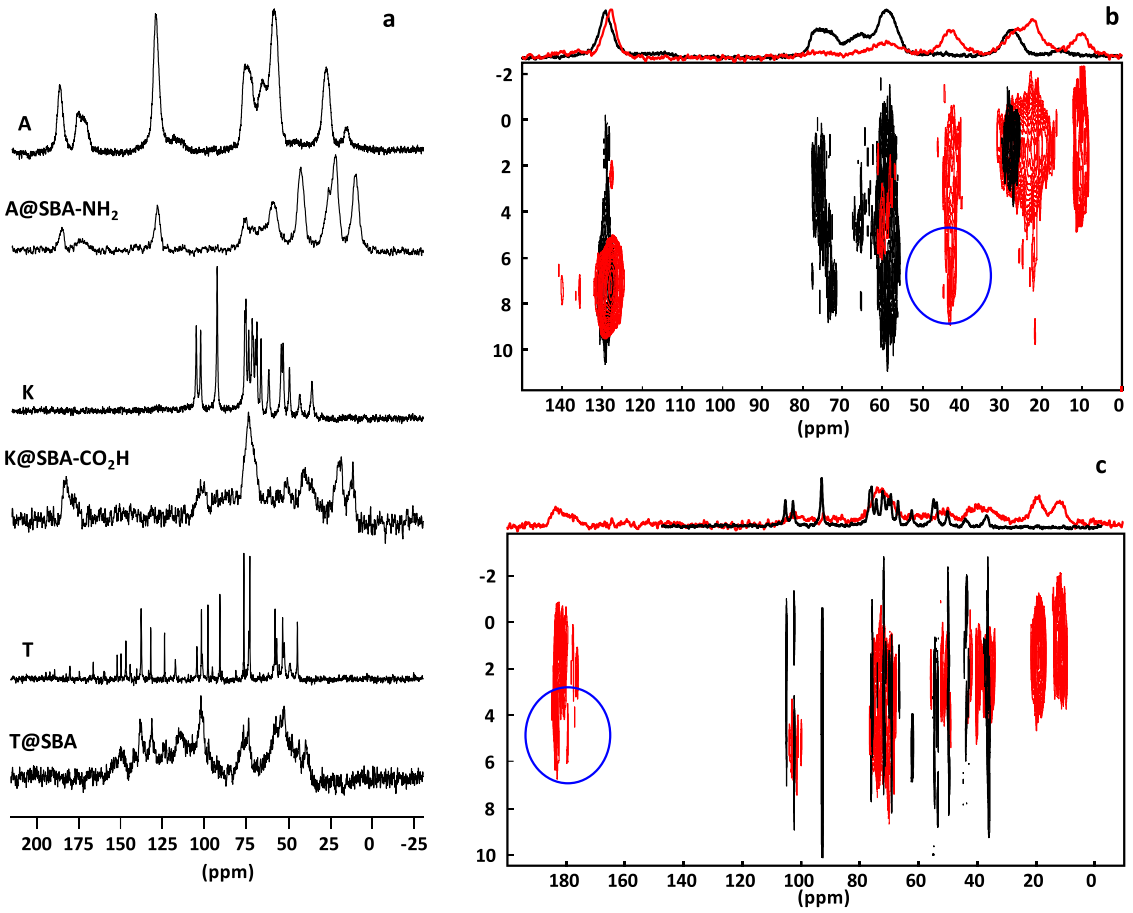

Figure 4. (a) ^{13}C CP MAS NMR spectra of pure drugs and drug-loaded systems. 2D HETCOR ^{13}C-{^{1}H} CP MAS NMR spectra of (b) ampicillin (black) and loaded A@SBA-NH_2 (red); (c) kanamycin (black) and loaded K@SBA-CO_2H. Blue circles show cross-peaks that can indicate the proximity between a carbon of the grafted spacer and a proton of the encapsulated drug (see text).

1520 cm^{-1} for N−H stretching vibrations, and 1450 cm^{-1} for OH bending.[22] The FTIR spectra of SBA change after drug loading. The characteristic bands of T are identified in the FTIR spectra of T@SBA, such as 1620 cm^{-1} for C=C, 1640 for C=O, 1500 cm^{-1} (smaller peak) for N-H, and 1460 cm^{-1} for OH bending. The C=O and N−H bands seem to shift to lower wavenumbers due to hydrogen bonding between carbonyl and amino groups of T molecules and SBA surface (smaller −OH deformation band at 1640 cm^{-1}).[22] This interaction can explain a lower amount of T in functionalized SBA because of a decrease of free silanol groups (Table S1).

Figure 5C exhibits the spectrum of the K molecule with the characteristic peaks at 1625, 1515, and 1190 cm^{-1}, assigned to the bending vibrations of the carbonyl stretching, amine bending, and alcohol, respectively.[45] The spectrum of the SBA-CO_2H carrier shows a band at 1713 cm^{-1} due to the C=O stretching frequency. Furthermore, it was confirmed by the band's absence at around 2250 cm^{-1} due to the −CN stretch that no unreacted cyano groups remained on the sample surface.[19,20] About the interaction between the carboxylic groups of the SBA-CO_2H carrier and the K molecules, further evidence can be obtained by comparing the FTIR spectra of the samples before and after impregnation, as illustrated in the magnification of the region 1800−1400 cm^{-1} (Figure 5D). In the FTIR spectrum of K@SBA-CO_2H, the carboxylic stretching vibration (1713 cm^{-1}) and N−H bending at 1515 cm^{-1} are no more observed. An intense carboxylate band at 1545 cm^{-1} is detected, suggesting that the $-COO^{-}$ NH_3^{+} bondings have formed between the $-NH_2$ groups of K molecules and the carboxylic groups of the SBA-CO_2H carrier.[20] As previously reported, a proton transfer between carboxylic groups and ammonia can be observed by FTIR spectroscopy.[19] Similarly, we also showed that the C=O stretching mode at 1713 cm^{-1} disappears, and a two-band appears at 1545 and 1407 cm^{-1} due to the carboxylate's ($-COO^{-}$) asymmetric and symmetric stretching vibrations, respectively.

The FTIR spectra of the A molecule, SBA-NH_2 carrier, and drug-loaded system (A@SBA-NH_2) are given in Figure 5E. Ampicillin sodium is a molecule that has carboxylate and amine functional groups. The typical FTIR bands of the ampicillin sodium spectrum shown in Figure 5E displays a broad, intense peak at 3300 cm^{-1} due to N−H stretching vibrations. The bands at 1767 and 1665 cm^{-1} were associated with C=O stretching vibrations, and aromatic ring chain C−C vibrations were observed at 1590 cm^{-1}.[46] The modification by amino groups of the SBA sample results in the appearance of the band at 1557 cm^{-1}, which is attributed to N−H stretching vibrations.[21,22,44] In the case of A@SBA-NH_2, the band at 1767 cm^{-1} disappeared completely (Figure 5F), which suggests that the A drug interacts through its carboxylate group ($-COO^{-}$) with SBA-NH_2. The peak at around 1540 cm^{-1} can be attributed to the interaction between the carboxylate group of the antibiotic and the amine group of the functionalized

https://doi.org/10.1021/acsomega.2c08065
ACS Omega 2023, 8, 12154−12164

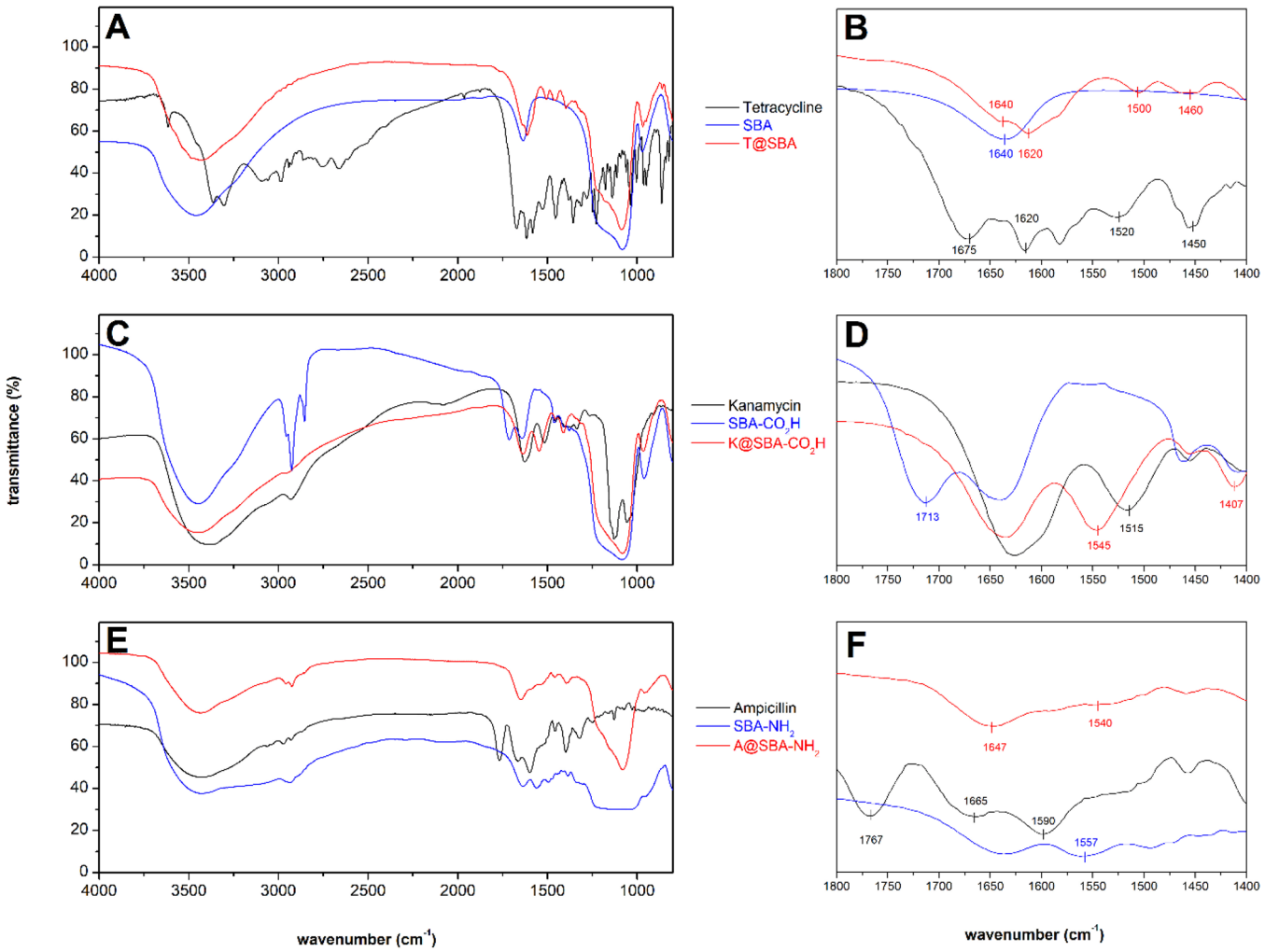

Figure 5. FTIR spectra of free drugs (solid black line), carriers (solid blue line), and drug-loaded systems (solid red line) in the 4000−800 cm^{-1} absorption region (A, C, and E) with a magnification of the region 1800−1400 cm^{-1} (B, D, and F).

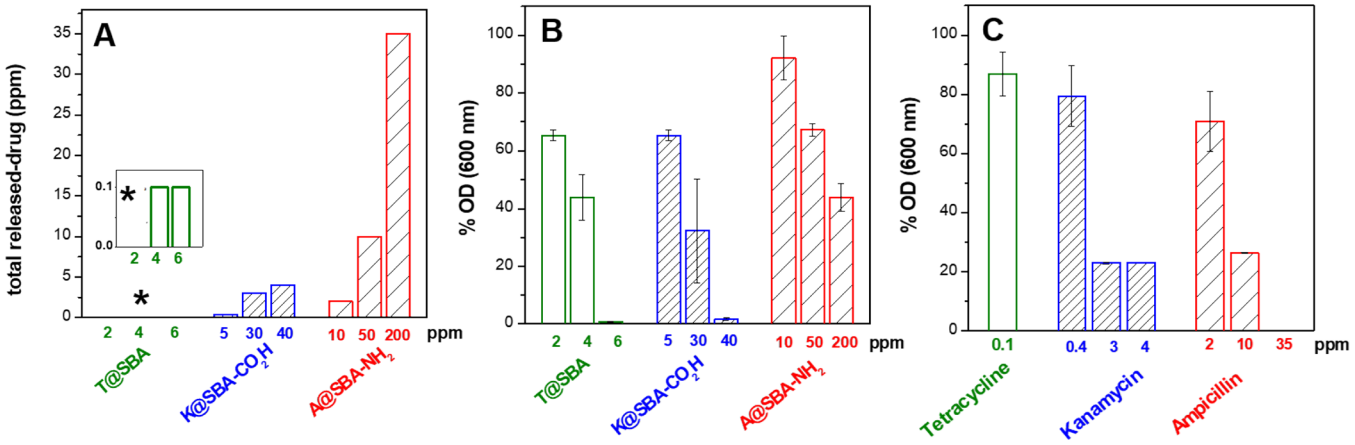

Figure 6. (A) Total released drug (in ppm, μg/mL) after 24 h of incubation at 37 °C in PB (0.1 M) at pH 7.4, from T@SBA (green bar), K@SBA-CO_2H (red bar), and A@SBA-NH_2 (blue bar). The calculation is based on a specified percentage obtained from the weight percentage of drug in the material, release experiments, and starting from x ppm of material (see sample concentration in ppm). Inset: zoom on total released T, as indicated by one asterisk. (B) Bar graphs illustrate the OD percentage (at 600 nm) of the surviving *E. coli* bacteria (DH5α) in the MHB medium alone as positive control and in the presence of the synthesized systems within the ppm concentration (μg/mL) range at distinct sample concentrations after 20 h of incubation. The quantification protocol used here is fully described in the Supporting Information. (C) OD percentage of surviving *E. coli* bacteria after 20 h exposure to free T, K, and A at distinct drug concentrations (in ppm). Error bars represent the standard deviation.

https://doi.org/10.1021/acsomega.2c08065
ACS Omega 2023, 8, 12154−12164

carrier, which reveals that the $-COO^-$ NH_3^+ bond is also present in A@SBA-NH_2. These observations confirm the ionic character of the drug@carrier interactions.[20,21,47]

Biological Experiments. *Release Experiments.* The T release experiments were performed by measuring the UV−vis spectroscopic signal of released T along distinct time intervals. The fluorescamine method was used to analyze the released K and A amount by fluorescence spectroscopy during delivery experiments.[24] Figure S6 presents the drug release evolution during the experiments. The release profiles and the total released drug of the systems are completely different. For T@SBA, K@SBA-CO_2H, and A@SBA-NH_2, the drug loadings are very similar (19.4, 16.5, and 17.4 wt %, respectively), and the functional groups loading in K@SBA-CO_2H and A@SBA-NH_2 are in the same order of magnitude (8 and 9 wt %, respectively). Thus, the organic loadings have a minimal effect on the in vitro release behavior. The nature of the drug and its interaction with the host matrix play a critical role in these different behaviors.

After 24 h of incubation at 37 °C in PB (0.1 M) at pH 7.4, the released drug was 87, 54, and 11 wt % of the total encapsulated drug for A@SBA-NH_2, K@SBA-CO_2H, and T@SBA, respectively. The result obtained for T@SBA correlates well with the data found in our previous study.[13] We then suggest that the micropore cavities retain a fraction of the T molecules. Contrarily, the total released T reached 94% in the MHB medium, suggesting that the drug leakage was facilitated. It is observed that the release profile of K@SBA-CO_2H is different from A@SBA-NH_2. Interestingly, unlike the release profiles of K@SBA-CO_2H, the release rate of A@SBA-NH_2 was very high, and the entrapped drug can be released entirely in only 1 h, which confirms a significantly easy A removal from the structure's outermost surface. In the release of K from the SBA-CO_2H carrier, there is an initial burst release in 8 h followed by a slow release. The initial burst release may be due to the excessive drug, which was weakly entrapped inside the mesopores or located at the outer surface of SBA-CO_2H. However, the smaller pore cavities might retain a fraction of the K molecules (see Figure 3C). After 8 h and the delivery of the adsorbed K on the outer surface, the slow release of the rest of the drug is attributed to a release of smaller pore-trapped K molecules. Figure 6A shows the total released drug (in ppm, μg/mL) after 24 h of incubation.

It is essential to mention that to build up our main conclusions properly, various concentrations (from 2 to 200 ppm) of the systems have been investigated for the in vitro release and bactericidal studies. Table S2 summarizes the total released drug in terms of ppm concentration. As shown in Figure 6A (inset), a maximum of 0.1 ppm of released T is reached up to 6 ppm of T@SBA. For K@SBA-CO_2H and A@SBA-NH_2 (Figure 6A), the total released drug can be further increased by increasing the concentration of the corresponding system. Consequently, the total released drug reached 4 ppm starting from 40 ppm of K@SBA-CO_2H and 35 ppm with 200 ppm of A@SBA-NH_2.

Antibacterial Activity against *E. coli* Bacteria. The antibacterial activity of the synthesized systems within the ppm concentration range at neutral pH was investigated against the susceptible *E. coli* strain (DH5α). Figure S7 shows the growth curves of *E. coli* bacteria growing in a 96-well plate in MHB bacterial medium alone as positive control and in the presence of synthesized systems and free drugs at distinct sample concentrations. Thereby, 1 ppm of tetracycline hydrochloride, 5 ppm of kanamycin sulfate, and 15 ppm of ampicillin sodium lead to the total death of the bacteria. Figure 6B presents percentages of OD (measured at 600 nm) of the positive control and systems incubated with bacteria. These percentages were obtained by comparing the OD measure of the systems with the positive control after 20 h of incubation. Thus, these data give the percentage of surviving bacteria at the end of the incubation experiments. All synthesized systems showed antibacterial activity from 2, 5, and 10 ppm for T@SBA, K@SBA-CO_2H, and A@SBA-NH_2, respectively. For each system, the toxicity increases while increasing their concentration. Due to a possible bactericidal activity of the carriers, the drug-unloaded systems' bactericidal effect was also evaluated (Figure S8) and no antibacterial activity was observed (concentrations used along these tests are related to the maximum amount of each corresponding drug-loaded system). Based on drug release experiments (Figure 6A), the T@SBA system exhibits the lowest released drug (0.1 ppm), and 6 ppm of that one leads to the total death of the bacteria. A tetracycline-containing MCM-41 mesoporous silica nanoparticle (with 19 wt % of tetracycline) showed inhibition on *E. coli* bacterial growth.[48] The percent survival of *E. coli* decreased to 3% in 4 h after treatment with a concentration material corresponding to 10 ppm of tetracycline. The significant improvement in antibacterial activity using 40 ppm of K@SBA-CO_2H and 200 ppm of A@SBA-NH_2 was due to higher K and A release rates (4 and 35 ppm, respectively, see Figure 6A).

The bactericidal efficiency of the synthesized systems was compared with that of free T, K, and A (Figure 6C). Drug concentrations used along these tests correspond to the maximum released amount of each drug starting from three significant concentrations of the synthesized systems (Figure 6A). Surprisingly, more viable *E. coli* were observed for free T (a value of 87% OD percentage of the surviving *E. coli* bacteria) and K (from 79 to 23%) when compared to T@SBA (from 65 to 0.8%) and K@SBA-CO_2H (from 65 to 1.6%) systems, respectively. Conversely, using 35 ppm of free A leads to total death of the bacteria, while 44% ($\pm$ 5%) of viable bacteria was observed with 200 ppm of A@SBA-NH_2. For free A, all the drug amount (35 ppm) was mixed with bacterial medium from the beginning of incubation. It is different when using 200 ppm of the A@SBA-NH_2 system that slowly releases A (35 ppm after 24 h) during incubation (Figure S6). In terms of bactericidal efficiency against susceptible *E. coli* strains (DH5α), free drugs followed the same order as the corresponding systems T > K > A.

CONCLUSIONS

SBA-15 was synthesized and modified with amino and carboxylic acid groups to optimize the loadings of tetracycline hydrochloride, kanamycin sulfate, and ampicillin sodium. NMR and FTIR experiments showed strong ionic interactions between modified silica surfaces and functional groups of kanamycin and ampicillin. In vitro release studies revealed that modified SBA had slower release rates than tetracycline-loaded unfunctionalized SBA. Total death of susceptible *E. coli* bacteria is obtained using a few ppm of tetracycline-loaded unfunctionalized SBA and kanamycin-loaded carboxylic acid-functionalized SBA, while ampicillin-loaded amino-functionalized-SBA exhibited lower bactericidal efficiency. These results demonstrate the high potential of the functional strategy used here to increase drug loading and control drug release. We foresee that these results will open a new area of

https://doi.org/10.1021/acsomega.2c08065
ACS Omega 2023, 8, 12154−12164

research where new biologically-active carriers will be designed and produced.

■ ASSOCIATED CONTENT

Supporting Information

The Supporting Information is available free of charge at https://pubs.acs.org/doi/10.1021/acsomega.2c08065.

Structures of tetracycline hydrochloride, kanamycin sulfate, and ampicillin sodium; TEM images of SBA-CO_2H and SBA-NH_2 carriers; TGA weight loss and weight percentage of organic groups (O) and drugs; calculated ^1H and ^{13}C NMR parameters in kanamycin monosulfate monohydrate (CCDC 1198235) and tentative assignment of the ^{13}C CP MAS NMR spectrum of kanamycin; calculated ^1H and ^{13}C NMR parameters in tetracycline hydrochloride (CCDC 153890) and tentative assignment of the ^{13}C CP MAS NMR spectrum of T; tentative assignment of the ^{13}C CP MAS NMR spectra of the free drugs, TGA weight loss, and weight percentage of organic groups and drugs; cumulative drug release from T@SBA, K@SBA-CO_2H, and A@SBA-NH_2; total released drug after 24 h of incubation; growth curves of *E. coli* bacteria growing in MHB bacterial medium of drug-(un)loaded synthesized systems and free drugs; growth curves of *E. coli* bacteria growing in a 96-well plate in MHB bacterial medium of drug-unloaded systems (PDF)

■ AUTHOR INFORMATION

Corresponding Author

Karim Bouchmella − *Brazilian Synchrotron Light Laboratory (LNLS), Brazilian Center for Research in Energy and Materials (CNPEM), Campinas CEP 13083-970 SP, Brazil; Chemistry Institute (IQ), Universidade Estadual de Campinas (UNICAMP), Campinas CEP 13083-970 SP, Brazil; ICGM, University Montpellier, CNRS, ENSCM, 34095 Montpellier, France;* orcid.org/0000-0002-8660-802X; Email: karim.bouchmella@umontpellier.fr

Authors

Quentin Lion − *Brazilian Synchrotron Light Laboratory (LNLS), Brazilian Center for Research in Energy and Materials (CNPEM), Campinas CEP 13083-970 SP, Brazil; Interdisciplinary Cluster for Applied Genoproteomics, Laboratory of Medical Chemistry, and GIGA Stem Cells, University of Liege, Liege 4000, Belgium;* orcid.org/0000-0002-9662-9318

Christel Gervais − *LCMCP - Laboratoire de Chimie de la Matière Condensée de Paris, Sorbonne Université, 75252 Paris Cedex 05, France;* orcid.org/0000-0001-7450-1738

Mateus Borba Cardoso − *Brazilian Synchrotron Light Laboratory (LNLS), Brazilian Center for Research in Energy and Materials (CNPEM), Campinas CEP 13083-970 SP, Brazil; Chemistry Institute (IQ), Universidade Estadual de Campinas (UNICAMP), Campinas CEP 13083-970 SP, Brazil;* orcid.org/0000-0003-2102-1225

Complete contact information is available at: https://pubs.acs.org/10.1021/acsomega.2c08065

Notes

The authors declare no competing financial interest.

■ ACKNOWLEDGMENTS

M.B.C. thanks the support of FAPESP (Grant Nos. 2014/22322-2, 2015/25406-5, and 2021/12071-6) and the productivity research fellowship granted by CNPq (Grant No. 309107/2014-8). K.B. and Q.L. acknowledge the support of Capes (CSF-PAJT - 88887.091023/2014-00). NMR spectroscopic calculations were performed using HPC resources from GENCI-IDRIS (Grant 097535). The French Région Ile de France-SESAME program is acknowledged for financial support (700 MHz spectrometer). The authors would like to thank LNLS and LNNano for all financial support along this work. D1B and D2A SAXS beamlines (LNLS-Brazil) are acknowledged for the usage of the SAXS beamlines. We thank Jessica Fernanda Affonso de Oliveira, Agustin S. Picco, and Murilo Izidoro Santos for fruitful insights in the fluorescence spectroscopy, bactericidal experiments, and drug derivatization for spectroscopic quantification. Pr Ahmad Mehdi is acknowledged for fruitful discussions. We thank Dr. Marcio Chaim Bajgelman (LNBio - Campinas, Brazil) for providing *E. coli* bacteria (DH5α) for biological assays.

■ REFERENCES

(1) Vallet-Regi, M.; Rámila, A.; del Real, R. P.; Pérez-Pariente, J. A New Property of MCM-41: Drug Delivery System. *Chem. Mater.* **2001**, *13*, 308−311.

(2) Vallet-Regí, M.; Balas, F.; Arcos, D. Mesoporous materials for drug delivery. *Angew. Chem., Int. Ed.* **2007**, *46*, 7548−7558.

(3) Wang, Y.; Zhao, Q.; Hu, Y.; Sun, L.; Bai, L.; Jiang, T.; Wang, S. Ordered nanoporous silica as carriers for improved delivery of water insoluble drugs: a comparative study between three dimensional and two dimensional macroporous silica. *Int. J. Nanomed.* **2012**, *8*, 4015−4031.

(4) Jain, K. K., Drug Delivery Systems - An Overview. In *Drug Delivery Systems*, Jain, K. K., Ed. Humana Press: Totowa, NJ, 2008; pp. 1−50, DOI: 10.1007/978-1-59745-210-6_1.

(5) Yoo, J.-W.; Irvine, D. J.; Discher, D. E.; Mitragotri, S. Bio-inspired, bioengineered and biomimetic drug delivery carriers. *Nat. Rev. Drug Discov.* **2011**, *10*, 521−535.

(6) Li, Z.; Barnes, J. C.; Bosoy, A.; Stoddart, J. F.; Zink, J. I. Mesoporous silica nanoparticles in biomedical applications. *Chem. Soc. Rev.* **2012**, *41*, 2590−2605.

(7) Manzano, M.; Vallet-Regí, M. New developments in ordered mesoporous materials for drug delivery. *J. Mater. Chem.* **2010**, *20*, 5593−5604.

(8) Wu, S.-H.; Hung, Y.; Mou, C.-Y. Mesoporous silica nanoparticles as nanocarriers. *Chem. Commun.* **2011**, *47*, 9972−9985.

(9) Bernardos, A.; Piacenza, E.; Sancenón, F.; Hamidi, M.; Maleki, A.; Turner, R. J.; Martínez-Máñez, R. Mesoporous Silica-Based Materials with Bactericidal Properties. *Small* **2019**, *15*, 1900669−1900702.

(10) Chircov, C.; Spoială, A.; Păun, C.; Crăciun, L.; Ficai, D.; Ficai, A.; Andronescu, E.; Turculeţ, Ş. C. Mesoporous Silica Platforms with Potential Applications in Release and Adsorption of Active Agents. *Molecules* **2020**, *25*, 3814−3848.

(11) Gaslain, F. O. M.; Delacôte, C.; Walcarius, A.; Lebeau, B. One-step preparation of thiol-modified mesoporous silica spheres with various functionalization levels and different pore structures. *J. Sol-Gel Sci. Technol.* **2009**, *49*, 112−124.

(12) Zapilko, C.; Widenmeyer, M.; Nagl, I.; Estler, F.; Anwander, R.; Raudaschl-Sieber, G.; Groeger, O.; Engelhardt, G. Advanced Surface Functionalization of Periodic Mesoporous Silica: Kinetic Control by Trisilazane Reagents. *J. Am. Chem. Soc.* **2006**, *128*, 16266−16276.

(13) Bouchmella, K.; Campanaro, F. D.; Mondo, G. B.; Santos, M. I.; Franco, C. H.; Moraes, C. B.; Biolley, C.; Mehdi, A.; Cardoso, M. B. Tetracycline@silver ions-functionalized mesoporous silica for high

bactericidal activity at ultra-low concentration. *Nanomedicine* **2018**, *13*, 1731−1751.
(14) Ritter, H.; Brühwiler, D. Accessibility of Amino Groups in Postsynthetically Modified Mesoporous Silica. *J. Phys. Chem. C* **2009**, *113*, 10667−10674.
(15) Crisci, A. J.; Tucker, M. H.; Lee, M.-Y.; Jang, S. G.; Dumesic, J. A.; Scott, S. L. Acid-Functionalized SBA-15-Type Silica Catalysts for Carbohydrate Dehydration. *ACS Catal.* **2011**, *1*, 719−728.
(16) Bonhomme, C.; Gervais, C.; Laurencin, D. Recent NMR developments applied to organic−inorganic materials. *Prog. Nucl. Magn. Reson. Spectrosc.* **2014**, *77*, 1−48.
(17) Azaïs, T.; Tourné-Péteilh, C.; Aussenac, F.; Baccile, N.; Coelho, C.; Devoisselle, J.-M.; Babonneau, F. Solid-State NMR Study of Ibuprofen Confined in MCM-41 Material. *Chem. Mat.* **2006**, *18*, 6382−6390.
(18) Azaïs, T.; Hartmeyer, G.; Quignard, S.; Laurent, G.; Tourné-Péteilh, C.; Devoisselle, J.-M.; Babonneau, F. Solid-state NMR characterization of drug-model molecules encapsulated in MCM-41 silica. *Pure Appl. Chem.* **2009**, *81*, 1345−1355.
(19) Fiorilli, S.; Onida, B.; Bonelli, B.; Garrone, E. In Situ Infrared Study of SBA-15 Functionalized with Carboxylic Groups Incorporated by a Co-condensation Route. *J. Phys. Chem. B* **2005**, *109*, 16725−16729.
(20) Tang, Q.; Xu, Y.; Wu, D.; Sun, Y. A study of carboxylic-modified mesoporous silica in controlled delivery for drug famotidine. *J. Solid State Chem.* **2006**, *179*, 1513−1520.
(21) Sevimli, F.; Yilmaz, A. Surface functionalization of SBA-15 particles for amoxicillin delivery. *Microporous Mesoporous Mater.* **2012**, *158*, 281−291.
(22) Hashemikia, S.; Hemmatinejad, N.; Ahmadi, E.; Montazer, M. Optimization of tetracycline hydrochloride adsorption on amino modified SBA-15 using response surface methodology. *J. Colloid Interface Sci.* **2015**, *443*, 105−114.
(23) Bibent, N.; Mehdi, A.; Silly, G.; Henn, F.; Devautour-Vinot, S. Proton Conductivity versus Acidic Strength of One-Pot Synthesized Acid-Functionalized SBA-15 Mesoporous Silica. *Eur. J. Inorg. Chem.* **2011**, *2011*, 3214−3225.
(24) Chen, Y.; Zhang, Y. Fluorescent quantification of amino groups on silica nanoparticle surfaces. *Anal. Bioanal. Chem.* **2011**, *399*, 2503−2509.
(25) Giannozzi, P.; Baroni, S.; Bonini, N.; Calandra, M.; Car, R.; Cavazzoni, C.; Ceresoli, D.; Chiarotti, G. L.; Cococcioni, M.; Dabo, I.; Dal Corso, A.; de Gironcoli, S.; Fabris, S.; Fratesi, G.; Gebauer, R.; Gerstmann, U.; Gougoussis, C.; Kokalj, A.; Lazzeri, M.; Martin-Samos, L.; Marzari, N.; Mauri, F.; Mazzarello, R.; Paolini, S.; Pasquarello, A.; Paulatto, L.; Sbraccia, C.; Scandolo, S.; Sclauzero, G.; Seitsonen, A. P.; Smogunov, A.; Umari, P.; Wentzcovitch, R. M. QUANTUM ESPRESSO: a modular and open-source software project for quantum simulations of materials. *J. Phys.: Condens. Matter* **2009**, *21*, 395502−395521.
(26) Perdew, J. P.; Burke, K.; Ernzerhof, M. Generalized Gradient Approximation Made Simple. *Phys. Rev. Lett.* **1996**, *77*, 3865−3868.
(27) Troullier, N.; Martins, J. L. Efficient pseudopotentials for plane-wave calculations. *Phys. Rev. B* **1991**, *43*, 1993−2006.
(28) Kleinman, L.; Bylander, D. M. Efficacious Form for Model Pseudopotentials. *Phys. Rev. Lett.* **1982**, *48*, 1425−1428.
(29) Pickard, C. J.; Mauri, F. All-electron magnetic response with pseudopotentials: NMR chemical shifts. *Phys. Rev. B* **2001**, *63*, 245101−245126.
(30) Zhao, D.; Huo, Q.; Feng, J.; Chmelka, B. F.; Stucky, G. D. Nonionic Triblock and Star Diblock Copolymer and Oligomeric Surfactant Syntheses of Highly Ordered, Hydrothermally Stable, Mesoporous Silica Structures. *J. Am. Chem. Soc.* **1998**, *120*, 6024−6036.
(31) Boullanger, A.; Gracy, G.; Bibent, N.; Devautour-Vinot, S.; Clément, S.; Mehdi, A. From an Octakis(3-cyanopropyl)-silsesquioxane Building Block to a Highly COOH-Functionalized Hybrid Organic−Inorganic Material. *Eur. J. Inorg. Chem.* **2012**, *2012*, 143−150.
(32) Barczak, M. Functionalization of mesoporous silica surface with carboxylic groups by Meldrum's acid and its application for sorption of proteins. *J. Porous Mater.* **2019**, *26*, 291−300.
(33) Cheik Ibrahim, A.; Meyer, M.; Devautour-Vinot, S.; Habas, J.-P.; Clément, S.; Naoufal, D.; Mehdi, A. A facile synthesis of proton-conducting organic-inorganic membranes. *J. Membr. Sci.* **2014**, *470*, 189−196.
(34) Gunathilake, C.; Dassanayake, R. S.; Abidi, N.; Jaroniec, M. Amidoxime-functionalized microcrystalline cellulose−mesoporous silica composites for carbon dioxide sorption at elevated temperatures. *J. Mater. Chem. A* **2016**, *4*, 4808−4819.
(35) Alauzun, J.; Mehdi, A.; Reyé, C.; Corriu, R. J. P. Direct synthesis of bifunctional mesoporous organosilicas containing chelating groups in the framework and reactive functional groups in the channel pores. *J. Mater. Chem.* **2007**, *17*, 349−356.
(36) Liu, M.; Hou, L.-a.; Yu, S.; Xi, B.; Zhao, Y.; Xia, X. MCM-41 impregnated with A zeolite precursor: Synthesis, characterization and tetracycline antibiotics removal from aqueous solution. *Chem. Eng. J.* **2013**, *223*, 678−687.
(37) Soni, S. S.; Brotons, G.; Bellour, M.; Narayanan, T.; Gibaud, A. Quantitative SAXS Analysis of the P123/Water/Ethanol Ternary Phase Diagram. *J. Phys. Chem. B* **2006**, *110*, 15157−15165.
(38) Asleson, G. L.; Frank, C. W. Carbon-13 nuclear magnetic resonance spectral analysis of tetracycline hydrochloride and related antibiotics. *J. Am. Chem. Soc.* **1975**, *97*, 6246−6248.
(39) Eneva, G. I.; Spassov, S. L.; Haimova, M. Complete 1H and 13C NMR assignments for kanamycin A, kanamycin B and penta-N-acetyl-kanamycin B. *Spectrochim. Acta, Part A* **1991**, *47*, 875−880.
(40) Antzutkin, O. N.; Lee, Y. K.; Levitt, M. H. 13C and15N - Chemical Shift Anisotropy of Ampicillin and Penicillin-V Studied by 2D-PASS and CP/MAS NMR. *J. Magn. Reson.* **1998**, *135*, 144−155.
(41) Kang, J.; Liu, H.; Zheng, Y.-M.; Qu, J.; Chen, J. P. Application of nuclear magnetic resonance spectroscopy, Fourier transform infrared spectroscopy, UV−Visible spectroscopy and kinetic modeling for elucidation of adsorption chemistry in uptake of tetracycline by zeolite beta. *J. Colloid Interface Sci.* **2011**, *354*, 261−267.
(42) Wang, H.; Gao, X.; Wang, Y.; Wang, J.; Niu, X.; Deng, X. Effect of amine functionalization of SBA-15 on controlled baicalin drug release. *Ceram. Int.* **2012**, *38*, 6931−6935.
(43) Kokunešoski, M.; Gulicovski, J.; Matović, B.; Logar, M.; Milonjić, S. K.; Babić, B. Synthesis and surface characterization of ordered mesoporous silica SBA-15. *Mater. Chem. Phys.* **2010**, *124*, 1248−1252.
(44) Szegedi, A.; Popova, M.; Goshev, I.; Mihaly, J. Effect of amine functionalization of spherical MCM-41 and SBA-15 on controlled drug release. *J. Solid State Chem.* **2011**, *184*, 1201−1207.
(45) Ilma, N.; Rizka, F. Quantitative vibrational methods development and its performance comparison to colorimetry on the assay of kanamycin sulfate. *Int. J. Appl. Pharm.* **2019**, *11*, 426−435.
(46) Sabitha, M.; Rajiv, S. Preparation and characterization of ampicillin-incorporated electrospun polyurethane scaffolds for wound healing and infection control. *Polym. Eng. Sci.* **2015**, *55*, 541−548.
(47) Moritz, M.; Łaniecki, M. SBA-15 mesoporous material modified with APTES as the carrier for 2-(3-benzoylphenyl)propionic acid. *Appl. Surf. Sci.* **2012**, *258*, 7523−7529.
(48) Koneru, B.; Shi, Y.; Wang, Y.-C.; Chavala, S.; Miller, M.; Holbert, B.; Conson, M.; Ni, A.; Di Pasqua, A. Tetracycline-Containing MCM-41 Mesoporous Silica Nanoparticles for the Treatment of Escherichia coli. *Molecules* **2015**, *20*, 19690−19698.

https://doi.org/10.1021/acsomega.2c08065
ACS Omega 2023, 8, 12154−12164